Quantitative Assessment of Nanoparticle Biodistribution by Fluorescence Imaging, Revisited

Fanfei Meng[1,2], **Jianping Wang**[1,2], **Qineng Ping**[2], and **Yoon Yeo**[1,3,*]

[1]Department of Industrial and Physical Pharmacy, Purdue University, 575 Stadium Mall Drive, West Lafayette, IN 47907, USA

[2]Department of Pharmaceutics, State Key Laboratory of Natural Medicines, China Pharmaceutical University, 24 Tong Jia Xiang, Nanjing 210009, China

[3]Weldon School of Biomedical Engineering, Purdue University, West Lafayette, IN 47907, USA

Abstract

Fluorescence-based whole body imaging is widely used in the evaluation of nanoparticles (NPs) in small animals, often combined with quantitative analysis to indicate their spatiotemporal distribution following systemic administration. An underlying assumption is that the fluorescence label represents NPs and the intensity increases with the amount of NPs and/or the labeling dyes accumulated in the region of interest. We prepare DiR-loaded poly(lactic-co-glycolic acid) (PLGA) NPs with different surface layers (polyethylene glycol with and without folate terminus) and compare the distribution of fluorescence signals in a mouse model of folate-receptor expressing tumor by near infrared fluorescence whole body imaging. Unexpectedly, we observe that fluorescence distribution patterns differ far more dramatically with DiR loading than with the surface ligand, reaching opposite conclusions with the same type of NPs (tumor-specific delivery *vs.* predominant liver accumulation). Analysis of DiR-loaded PLGA NPs reveal that fluorescence quenching, dequenching and signal saturation, which occur with the increasing dye content and local NP concentration, are responsible for the conflicting interpretations. This study highlights the critical need for validating fluorescence labeling of NPs in the quantitative analysis of whole body imaging. In light of our observation, we make suggestions for future whole body fluorescence imaging in the *in vivo* evaluation of NP behaviors.

Keywords

Whole body imaging; fluorescence quenching; fluorescence saturation; nanoparticles; biodistribution

---

Fluorescence-based whole body imaging is widely used in the evaluation of nanoparticle (NP) distribution in small animals. Fluorescence whole body imaging enables time-, labor- and cost-effective, non-invasive, and simple detection of NPs with a minimal number of required subjects.[1] Furthermore, fluorescence imaging can visualize spatiotemporal

---

*Corresponding author: Yoon Yeo, Ph.D., Phone: 1.765.496.9608, Fax: 1.765.494.6545, yyeo@purdue.edu.

distribution of NPs in the same animal, thereby reducing the inter-subject variability and enabling intuitive appreciation of the result.

For whole body imaging of NP distribution, NPs are labeled with fluorescent dyes *via* physical encapsulation or covalent conjugation. Fluorescence probes with absorption and emission wavelengths in the near-infrared (NIR) spectrum (650-900 nm) are most useful for whole body imaging, because NIR light can penetrate deep into the tissues[2-5] and tissues have minimal background interference in this region.[6,7] In particular, organic NIR fluorophores, especially cyanine dyes, are most commonly used due to the flexibility in controlling absorption wavelength and emission brightness.[4,8] Representative NIR cyanine dyes include indocyanine green (ICG), a US Food and Drug Administration–approved dye, [9,10] and 1,1′-dioctadecyl-3,3,3′,3′-tetramethylindotricarbocyanine iodide (DiR), a hydrophobic long-chain dialkylcarbocyanine. While both dyes can be physically encapsulated in NPs, ICG does not serve as a reliable probe of NPs as DiR *in vivo*. Being relatively hydrophilic, ICG is not stably retained in hydrophobic matrix such as poly(lactic-co-glycolic acid) (PLGA)[11] and lipid NPs[12] in circulation. Once released, ICG binds to serum proteins and emits stronger fluorescence than the dyes in NPs,[13] interfering with the tracking of ICG-loaded NPs.[14] In contrast, hydrophobic DiR is easily encapsulated and retained in various NPs, such as polymeric micelles,[15] liposomes,[16] exosomes,[17] polymeric particles,[18] and solid lipid particles.[19] Moreover, free DiR molecules in aqueous medium exhibit very weak fluorescence signal and do not override the NP signal in circulation.[20,21] Therefore, DiR has been a popular choice of tracer in fluorescent imaging of NP distribution. Since 2006, more than 2000 research articles have reported distribution patterns and kinetics of NP drug carriers using DiR as a fluorescence probe, according to a Google Scholar search run with "DiR dye nanoparticles distribution" as keywords.

In this study, we evaluate *in vivo* distribution of polymeric NPs in mice by NIR-fluorescence whole body imaging using DiR as a tracer of NPs. PLGA NPs are surface-modified with folate-conjugated polyethylene glycol (pFol) or methoxy-terminated polyethylene glycol (PEG) *via* polymerized tannic acid (pTA) as an intermediate adhesive layer. For evaluation of folate-dependent distribution of pFol-modified PLGA NPs, the NPs are loaded with DiR and injected intravenously (IV) to animals with folate receptor-overexpressing tumors. Surprisingly, the fluorescence distribution patterns differ far more dramatically with the DiR loading content than with the surface ligand, leading to opposite conclusions with the same type of NPs. We investigate the fluorescence properties of DiR-loaded PLGA NPs varying the DiR content and NP concentration and identify two distinct behaviors--quenching and saturation--that can affect the *in vivo* fluorescence kinetics and intensity profiles. In light of the potential artifacts, we revisit the imaging results and discuss its implication in the interpretation of whole body imaging. Our finding may be applicable to other fluorescent dyes used in whole body imaging and may explain, at least partly, the unresolved gap between the preclinical proof of concept and the clinical utility of nanomedicine. On the basis of our observation, we make suggestions for future *in vivo* fluorescence imaging studies.

Results and discussion

Encapsulated DiR represents NPs in serum.

To track the distribution of NPs in different organs by fluorescence imaging, NPs were labeled by encapsulation of NIR fluorescent dyes. We considered ICG and DiR based on their prevalent use in the literature for whole-body imaging.[22,23] Both NPs showed constant fluorescence in phosphate buffered saline (PBS, pH 7.4) over 6 h (duration of the observation) without spilling the fluorescence in the buffer. Upon incubation in mouse serum, ICG was quickly released from the NPs and detected in the supernatant as early as in 10 min, whereas DiR was stably retained in the NPs over 6 h (duration of the observation) (Figure S1). Free DiR dispersed in mouse serum showed no fluorescence (Figure S2) due to the formation of H-aggregates.[21, 24-26] These results indicate that DiR fluorescence can represent NPs in physiological fluid such as serum and blood. Therefore, DiR was chosen as a fluorescence marker of NPs for tracking their distribution in tumor-bearing mice.

Surface-modified PLGA NPs were prepared by the tannic acid-iron complexation method.

PLGA NPs encapsulating DiR (DiR/np) were prepared by the single emulsion method. PLGA was mixed with DiR (0.5 or 3.6 wt% of PLGA) in dichloromethane (DCM) and emulsified in water solution to form NPs, referred to as $DiR_{0.5}$/np or $DiR_{3.6}$/np according to the target DiR loading. The surface of DiR/np were modified with two different layers (pFol and mPEG) by the tannic acid-iron complexation (pTA) method.[27] Tannic acid forms a multivalent coordination bonding with Fe^{3+}, adsorbs to the surface of NPs and makes a thin pTA film, which can accommodate thiol- or amine-terminated functional ligands by Michael addition or Schiff base reactions.[28-30] The pTA was identified as a wrinkled layer on NP surface in transmission electron microscopy (TEM) images (Figure S3). pFol and mPEG were conjugated to the pTA-coated DiR/np (DiR/np-pTA) *via* the amine terminus to form DiR/np-pTA-pFol and DiR/np-pTA-PEG, respectively. The conjugation of pFol and mPEG was confirmed by matrix-assisted laser desorption/ionization-mass spectrometry (MALDI-MS). np-pTA-pFol and np-pTA-PEG were treated with trifluoroacetic acid to disassemble pTA and release pFol and mPEG. MALDI-MS detected the released pFol and mPEG at a m/z of 5000, identical to the original counterparts (Figure S4). Reflecting the difference of surface layers, np*-pTA-pFol and np*-pTA-PEG (rhodamine-labeled NPs) showed differential interaction with folate receptor-overexpressing KB cells. This difference disappeared upon co-treatment of extra folate (1 mM), confirming that the interaction between np*-pTA-pFol and KB cells were mediated by the folate receptor (Figure S5).

Due to the common core (PLGA NPs), the two NPs showed comparable particle sizes and morphology (Table S1 and Figure S3). According to the TEM images, the NPs had similar sizes ranging from 80 to 120 nm, irrespective of the dye loading and surface modification. DLS showed slightly larger sizes. The size difference between TEM and DLS measurements was greater than the thickness of the hydrated PEG layer, which is no more than a few nanometers.[31] This suggests that the NPs, especially those made with 3.6 wt% DiR loading, underwent a mild degree of aggregation in the buffer in which the NP size was measured. These aggregates resolved in 50% serum to individual NPs (Figure S6), indicating that the NPs would circulate with a similar size irrespective of the surface layer or the dye content.

Whole body fluorescence imaging exhibits conflicting NP distribution patterns in tumor-bearing mice.

The *in vivo* distribution patterns of DiR/np-pTA-pFol and DiR/np-pTA-PEG were examined in nude mice bearing subcutaneous KB tumors. Prior to the injection, we confirmed that both NPs, at 1 mg/mL, maintained stable fluorescence intensity in undiluted mouse serum over 72 h (Fig. 1, Fig. S7). DiR/np-pTA-pFol and DiR/np-pTA-PEG were administered in two DiR loadings (3.6 and 0.5 wt%; called $DiR_{3.6}$/NPs and $DiR_{0.5}$/NPs, collectively) and two NP doses (4 mg and 0.4 mg per mouse) with an expectation that a greater amount of dye and NPs would yield brighter signals in whole body imaging.

Animals receiving 0.4 mg of $DiR_{0.5}$/NPs (*i.e.*, 0.5% * 0.4 mg), irrespective of the NP type, showed weak fluorescence signal in the liver and spleen and no signal in tumor, likely due to the insufficient amount of dye in the system (Fig. 2). With 4 mg of NPs per mouse, bright signals were observed in the liver, spleen, tumor, and adipose fat pad in the buttock. In general, DiR/np-pTA-pFol showed greater fluorescence intensity in KB tumors than DiR/np-pTA-PEG (Fig. 2) as expected from the *in vitro* study (Figure S5). On the other hand, an intriguing, rather surprising trend was observed with different DiR loadings. Irrespective of the surface layer, $DiR_{0.5}$/NPs (0.5% * 4 mg) showed much brighter fluorescence signal in the liver than in tumor. In contrast, $DiR_{3.6}$/NPs (3.6% * 4 mg) showed ever-increasing fluorescence signal in tumor over 72 h (with a steeper slope than $DiR_{0.5}$/NPs), far exceeding the intensity in the liver (Fig. 2, Figure S8). Consequently, the ratio of tumor to liver signal (tumor/liver), an indicator of tumor-specific NP delivery relative to the reticuloendothelial (RES) organs, was much higher with $DiR_{3.6}$/NPs (3.6% * 4 mg) than with $DiR_{0.5}$/NPs (0.5% * 4 mg) (Fig. 3). With 3.6% * 4 mg, the tumor/liver ratio of DiR/np-pTA-pFol was greater than 1 from the initial time point and continued to increase, and that of DiR/np-pTA-PEG approached 1 at later time points. However, 0.5% * 4 mg showed rather constant tumor/liver ratios, lower than 0.5 for both DiR/np-pTA-pFol and DiR/np-pTA-PEG. *Ex vivo* imaging of excised organs showed a consistent trend. With $DiR_{0.5}$/NPs, tumor showed much lower fluorescence signal than the liver irrespective of the NP dose (0.5% * 0.4 mg and 0.5% * 4 mg). On the other hand, $DiR_{3.6}$/NPs (3.6% * 4 mg) exhibited brighter fluorescence signal in tumor than in the liver (DiR/np-pTA-pFol) or at least comparable signal to the liver (DiR/np-pTA-PEG) (Fig. 4).

For a selected treatment ($DiR_{0.5}$/np-pTA-pFol, 4 mg NPs per mouse: *i.e.*, 0.5% * 4 mg), we compared the tumor/liver ratio of *ex vivo* DiR signals and the ratio of DiR amounts determined by liquid-liquid extraction (LLE) of tissue lysates (a common practice of drug biodistribution studies). The tumor/liver ratio based on *ex vivo* images was dramatically higher than the ratio obtained from DiR extraction (Fig. 5). This result suggests that *ex vivo* imaging overestimate NP delivery to tumor relative to the liver.

The *in vivo* and *ex vivo* imaging was repeated additional three times with selected sets of NP dose and dye loading. The results consistently showed that NP distribution patterns observed by optical imaging differed according to the dye loading (Figure S9-S18). $DiR_{3.6}$/NPs showed selective increase of tumor signal and an ever-increasing ratio of tumor/liver signals (1) over time, and $DiR_{0.5}$/NPs maintained relatively stable and low tumor/liver ratio (<0.5).

The tumor/liver ratio measured by *ex vivo* imaging was much higher than that measured by LLE (Figure S18).

DiR-loaded NPs show fluorescence quenching and signal saturation.

The above results show that NPs with the same size and surface layer can exhibit very different patterns in whole body fluorescence imaging according to the dye loading, leading to conflicting interpretations of NP distribution (tumor-specific delivery *vs.* predominant liver accumulation). To investigate the effect of dye loading on the fluorescence intensity of NPs, we prepared DiR/np with different DiR loadings, suspended them in undiluted mouse serum at different concentrations (0-20 mg/mL), and measured the fluorescence intensity of the suspensions.

Two distinct trends were observed. First, their fluorescence intensity increased with the NP concentration over a narrow range but reached a plateau (**saturated**) at higher concentrations (Fig. 6a, Fig. S19). The concentration at which the fluorescence intensity saturated varied with the DiR loading: DiR/np with higher DiR loading showed the fluorescence saturation at lower NP concentrations (4 mg/mL for DiR_1/np; 2 mg/mL for $DiR_{3.6}$/np), whereas those with lower DiR loading did at higher concentrations (20 mg/mL for $DiR_{0.2}$/np; 10 mg/mL for $DiR_{0.5}$/np). Second, at relatively high NP concentrations (>2 mg/mL), the fluorescence intensity did not increase with the DiR loading but rather decreased. At NP concentrations higher than 8 mg/mL, DiR/np with the lowest DiR loading showed greatest fluorescence intensity and vice versa (Fig. 6a, Figure S20), suggesting that the concentrated dye molecules in the NPs have undergone **fluorescence quenching** due to the *intra*-particle dye interactions.[21,32] The fact that this inverse trend was seen at relatively high NP concentrations indicates that the increased *inter*-particle interactions also contributed to the quenching. To confirm the fluorescence quenching of DiR-loaded NPs, we examined the fluorescence intensity of the two NPs used in the animal studies (DiR/np-pTA-pFol and DiR/np-pTA-PEG). Consistent with the DiR/np, both NPs showed much lower fluorescence intensity with 3.6% DiR loading than with 0.5% (Fig. 6b) at the same NP concentration.

Given the potential of fluorescence quenching, the stability of NP fluorescence intensity in undiluted mouse serum was reexamined at different NP concentrations. $DiR_{3.6}$/np, which exhibited clear signs of fluorescence quenching at 4 mg/mL (Fig. 6a), showed increasing fluorescence intensity over 72 h when incubated at 5 or 20 mg/mL. The increasing fluorescence intensity of $DiR_{3.6}$/np is attributable to the release of DiR (by diffusion and NP degradation), which leads to the reduction of dye content in the NPs (*i.e.*, **dequenching**) over time. Interestingly, $DiR_{3.6}$/np at 20 mg/mL showed relatively mild dequenching, appearing darker than those at 5 mg/mL at all time points (Fig 7a, Fig. S21). This result may be explained by the low saturation solubility of DiR in aqueous medium (< 1 μg/mL in water[21]), which limits the release of the dye from the NPs. This is analogous to the drug release from NP formulations in a non-sink condition, which leads to a severe underestimation of the drug release kinetics.[33] On the other hand, $DiR_{3.6}$/np at 1 mg/mL maintained the constant fluorescence intensity over time, as previously observed with surface modified NPs (Fig. 1). This may be explained by the fact that $DiR_{3.6}$/np at 1 mg/mL was relatively less quenched due to the lower NP concentration, *i.e.*, lower *inter*-particle

interactions. Had a minor degree of dequenching occurred with DiR release, it might have been offset by the fluorescence reduction due to the loss of DiR. $DiR_{0.5}$/np also underwent dequenching over time at 20 mg/mL (Fig. 7b, Fig. S22). Those incubated at 1 and 5 mg/mL $DiR_{0.5}$/np showed constant fluorescence intensity over 72 h, most likely with a similar reason as 1 mg/mL $DiR_{3.6}$/np.

In summary, these results demonstrate that DiR-loaded NPs can undergo fluorescence quenching due to the dye interactions within the NPs (*intra*-particle dye interaction), which increases with the dye content in NPs, as well as the interactions between the NPs (*inter*-particle dye interaction), which increases with the NP concentration. The DiR-loaded NPs incubated in serum can show increasing fluorescence with time due to the decreasing dye interactions by the dye release (dequenching). The extent of dequenching varies with the dye concentration in the system, which depends on both dye loading and NP concentration. In addition, the fluorescence intensity of DiR-loaded NP suspension does not increase linearly with the NP concentration (fluorescence saturation), typical of fluorescent compounds.[34,35] The fluorescence quenching, differential dequenching, and saturation may explain the conflicting *in vivo* imaging results described previously.

Fluorescence quenching and dequenching interfere with the observation of NP accumulation in organs.

A notable observation in the whole body fluorescence imaging was that the NP signals in tumor increased more steeply with 3.6% DiR loading than with 0.5% over time for both types of NPs (Fig. 3 top, Figures S10, S13 and S16 top). The compared NPs ($DiR_{0.5}$/np-pTA-pFol (or -PEG) *vs.* $DiR_{3.6}$/np-pTA-pFol (or -PEG)) share similar size and surface layer and thus expected to show comparable biodistribution patterns. Therefore, the differential fluorescence increase cannot simply be interpreted as a difference in NP accumulation. We instead suspect that the signal increase may partly be attributable to gradual dequenching of the fluorescence, the extent of which varies with the dye loading. While dequenching may occur with both 0.5% and 3.6% loading (Fig. 7), the fluorescence in $DiR_{3.6}$/NPs are more quenched than $DiR_{0.5}$/NPs due to the concentrated dye (Fig. 6) and can thus be dequenched to a greater extent displaying a steeper increase in fluorescence intensity. Cho *et al.* also reported that polymeric micelles with a relatively high DiR/polymer ratio showed increasing fluorescence intensity in tumor over time while the micelles with a lower DiR/polymer ratio showed the opposite trend, suggesting the potential of DiR quenching and dequenching in the micelles.[21] From the imaging data alone, we cannot determine the extent to which the fluorescence dequenching contributed to the signal increase. However, it is clear that dequenching interferes with the observation of NP accumulation in organs. Therefore, when there is even a remote chance of fluorescence quenching in the dye-loaded NPs, one cannot tell whether the increase of fluorescence intensity is due to the accumulation of NPs in the tissue or the fluorescence dequenching by dye release and/or NP removal, which are in fact the opposite phenomena.

DiR in NPs can undergo differential dequenching according to NP concentration in each tissue, resulting in an exaggerated tumor/liver signal ratio.

The most intriguing observation was that $DiR_{3.6}$/NPs showed brighter fluorescence signals in the tumor than in the liver, whereas $DiR_{0.5}$/NPs showed a reverse trend (Figs. 2 and 3). This difference clearly and consistently manifested in the tumor/liver ratio of fluorescence signals: $DiR_{3.6}$/NPs showed an ever-increasing tumor/liver ratio of 1 for most of the time, whereas $DiR_{0.5}$/NPs showed a constant tumor/liver ratio of less than 0.5. This means that, with the NPs of the same size, matrix, surface layer and dose, one may make opposite interpretations of NP tissue distribution patterns, depending on the DiR loading. With $DiR_{3.6}$/NPs, one may conclude that the NPs tend to accumulate more in the tumor than in the liver over time. However, $DiR_{0.5}$/NPs may lead to a conclusion that the NPs accumulate consistently less in tumor than in the liver.

It is well known that NPs are delivered much less to the tumor as compared to the liver: typically, <5% of injected dose (ID) of NPs accumulate per gram of tumor (%ID/g), whereas 10-40% ID/g does in the liver.[36-40] Given this, the tumor/liver ratio greater than 1 seen with $DiR_{3.6}$/NPs is unusual. We speculate that the high tumor/liver ratio results from differential dequenching of $DiR_{3.6}$/NPs in liver and tumor (*i.e.*, more efficient dequenching in tumor than in liver) rather than the ratio of NP contents in those tissues. As shown in Fig. 7, the extent of dequenching depends on the concentration of NPs, especially with the high DiR loading. With the high NP concentration in the liver tissue, the hydrophobic DiR may not have been efficiently released from $DiR_{3.6}$/NPs. In contrast, the release of DiR in tumors would have been less restricted due to the relatively low NP concentration, resulting in more efficient dequenching than in the liver. On the other hand, $DiR_{0.5}$/NPs would have faced less limitation in dye release irrespective of the location due to the lower DiR concentration and thus have maintained a stable tumor/liver ratio at 0.5, consistent with typical NP distribution patterns.[41,42]

Fluorescence signal saturation leads to overestimation of NP delivery to tumors.

The *ex vivo* fluorescence signal of $DiR_{0.5}$/np-pTA-pFol in tumor relative to the liver was much higher than the ratio determined by LLE of the dye (Fig. 5). With *ex vivo* imaging the tumor/liver signal ratio was 0.21, but the ratio determined by LLE was 0.022, 10 times lower than the former. This difference can be explained by the non-linear relationship between the fluorescence intensity and NP concentration. We showed that the fluorescence intensity of $DiR_{0.5}$/NP suspended in mouse serum started to saturate at a concentration greater than 8 mg/mL. With NPs showing signal saturation, the NP content in the organs with relatively high NP concentration (*i.e.*, liver) is underestimated than the NPs at lower concentrations (*i.e.*, in tumor), leading to the exaggeration of the tumor/liver ratio. However, when the NP content is estimated by LLE of DiR, the concentration is determined against a calibration curve with a linear concentration *vs.* signal relationship, which eliminates the potential for underestimation. The LLE is a traditional practice of drug biodistribution studies and reflects the actual concentration of dyes delivered by the NPs. The tumor/liver ratio determined by the LLE method (0.022) is consistent with other studies that report dominant liver accumulation of drug delivered by NPs than tumor delivery.[36-40] This result demonstrates

that the fluorescence imaging can underestimate the NP signals in the organs where the NPs tend to be concentrated and thus overestimate the tumor signals relative to other organs.

Suggestions for future whole body fluorescence imaging.

DiR is widely used as a fluorescent tracer in whole body fluorescence imaging to assess the biodistribution and pharmacokinetics of nanomedicine. From 2017 to March 2018, 214 research articles have been published using DiR as a tracer of NPs, according to the Google Scholar. Of the 214 articles, 72 (34%) use the imaging for visual (qualitative) demonstration of NP distribution and 98 (46%) quantify the fluorescence intensity of the images, referring to the whole body imaging as "biodistribution" study. 39 articles (18%) quantify the *in situ* fluorescence intensity at different time points and interpret it as changes in the amount of NPs (or the dye delivered by the NPs) in each tissue or organ. Only 5 articles (2.3%) quantify the dye by traditional methods such as LLE.

Notwithstanding, our results demonstrate that (i) the increase of fluorescence intensity does not necessarily represent the NP accumulation in the organs; (ii) the relative fluorescence intensity between organs can be significantly affected by the dye content in the NPs (*i.e.*, quenching status) and the NP concentration in each organ, even leading to opposite conclusions with the same type of NPs; and (iii) the imaging analysis can overestimate the tumor/liver ratio of NP delivery. We reason that the fluorescence quenching/dequenching and saturation are responsible for the conflicting observations. Although our study was performed with DiR, the quenching and saturation issues are not limited to this particular dye. Most of the commonly used organic fluorescence dyes undergo aggregation-caused quenching and show decreasing fluorescence intensity with increasing concentrations. The quenching phenomenon is particularly serious for dyes with the emission wavelength in the far-red/NIR zone, because the elongated conjugation in large aromatic rings of NIR dyes make them more easily aggregate through π-π stacking.[43,44] For example, ICG and FPI-749 (equivalent to Cy7), commonly used as NP tracers in NIR *in vivo* imaging, show severe reduction in fluorescence intensity at high concentrations in mouse serum (Figure S23). The limitations of organic fluorescent dyes underscore the need for new imaging probes with improved optical properties. For example, inorganic chromophores such as quantum dots[45,46] and their organic counterparts (carbon dots[47]) have clear advantages in quantum yield and signal stability.[48] Traditional organic dyes continue to be valuable tools for the convenience and commercial availability, but it is important to recognize the signal quenching and saturation as prevalent issues and take necessary cautions. We suggest the following for the future whole body fluorescence imaging to avoid misinterpretation.

Mind quenching: Dye loading in NPs should be carefully validated.—It is tempting to increase the dye loading in NPs for the sake of the detection sensitivity. However, the fluorescence intensity of dye-loaded NPs does not necessarily increase with the dye content in NPs. To the contrary, the concentrated dye molecules will face an increasing chance of aggregation-caused quenching[8,32] and appear darker in the imaging (Fig. 6). More importantly, the dye in the quenched state exhibit increasing fluorescence intensity as it is removed from the tissues (by dye release and/or NP washout) and dequenched, belying the actual dye concentration in the tissue of interest. If the dequenching

occurs at different rates according to the NP concentration (Fig. 7a), the ratio of fluorescence intensity between different tissues is not only irrelevant but completely opposite to the relative NP delivery (low NP ratio = high fluorescence ratio). Therefore, in order to use the fluorescence intensity for assessing relative NP biodistribution, it is necessary to confirm that the dye molecules in the NPs are not in the quenched state. This can be done by titrating the dye loading, finding a range that does not show quenching (*i.e.*, fluorescence intensity increasing in proportion to dye loading), and ensuring that the dye content falls in this range. Since fluorescence quenching is increasingly evident in concentrated NP suspension (Fig. 6a and Figure S20), the dose screening should be performed over a broad range of NP concentrations.

Fluorescence quenching between adjacent fluorophores (within 10 nm) is a very well-known phenomenon[49-51] and has actively been used for diagnostics.[52,53] For example, a NIR fluorophore conjugated to a synthetic polymer *via* an enzyme-sensitive peptide linker was used as an imaging probe for enzyme detection, where the enzyme-sensitive cleavage of the linker induces the fluorophore release and the fluorescence increase (*i.e.*, dequenching).[54] However, the potential of fluorescence quenching and its implication in the interpretation of the fluorescence change are seldom considered in the image-based analysis of NP distribution. Moreover, the method description of an article provides little information for the readers to judge the potential of quenching. The consequence of misinterpreted imaging is grave: if one used $DiR_{3.6}$/NPs of our study without validating the quenching status, one may conclude that the NPs have been well "targeted" to tumors with minimal liver accumulation, when in reality the NPs may well have accumulated in the liver far more than in the tumor.

Mind saturation: tumor/liver signal ratio can be overestimated due to saturation.

—*In situ* or *ex vivo* imaging simplifies the quantification of NPs and eliminates the labor-intensive tissue preparation and extraction processes. However, it is important to keep it in mind that quantitative comparison of fluorescence intensity is meaningful only when there is a linear relationship between fluorescence intensity and the NP concentration. The signal saturation of fluorescent compounds is a prevalent phenomenon. When fluorescent compounds are used for quantification, one knows to dilute the samples to make their signals fall within the linear range. However, it is difficult to calibrate and validate the linearity of signals with *in situ* and *ex vivo* biological specimens. The fluorescence intensity in animal imaging is thus presented with a notion that it is at best semi-quantitative; nevertheless, with convoluted data processing such as normalization and ratio calculation, such a notion is often lost in translation and only the processed numbers remain to mislead the conclusion. In our example, even with $DiR_{0.5}$/NPs undergoing relatively low quenching in the liver, the tumor/liver signal ratio was 10 times higher than the tissue concentration ratio determined by LLE, due to the saturated fluorescence signal in the liver (Fig 5 and Fig S18). To avoid this, it will be ideal to validate the linearity of the signal-to-concentration relationship *in vivo* and ensure that the signals from the RES organs fall within the linear range. In this regard, it is beneficial to load a minimum amount of dye in the NPs as the NPs with lower dye loading have a broader range of linear signal-to-concentration relationship (Fig. 6a). If *in vivo* calibration is practically difficult, one should at least clarify that the

fluorescence imaging is only semi-quantitative and does not replace traditional biodistribution studies.

Conclusion

Whole body animal fluorescence imaging based on NIR fluorescence is widely used to monitor *in vivo* distribution of nanomedicine. The NIR fluorescence imaging has several advantages over traditional biodistribution studies, such as time- and cost-effectiveness, non-invasiveness, and simple detection. However, concentrated fluorescent dyes are prone to quenching and the signals of labeled NPs can saturate as the concentration increases. With two types of DiR-loaded PLGA NPs (DiR/np-pTA-pFol and DiR/np-pTA-PEG), we demonstrate that the same type of NPs may lead to very different interpretations of NP distribution depending on the dye loading content. At least three events can affect the data interpretation: (i) Fluorescence quenching and dequenching, which occur more severely with high DiR loading, interfere with the interpretation of fluorescence signal increase. (ii) For NPs with dyes in quenched state, fluorescence dequenching can occur at different rates according to the NP concentration in tissues, misleading the comparison of NP delivery between the tissues. (iii) Even with NPs of lower DiR loading (hence less chance of quenching), the fluorescence signal saturation can result in overestimation of NP delivery to tumors relative to the RES organs. To avoid misleading observations in whole body fluorescence imaging of NP distribution, it is important to validate that fluorescence dyes do not quench in NPs and the fluorescence intensity increases linearly with the NP concentration.

Materials and Methods

Materials

PLGA (LA:GA = 85:15, acid endcap, 150 kDa), FPI-749, and PLGA-rhodamine B conjugate (LA:GA = 50:50, 30 kDa) were purchased from Akina Inc. (West Lafayette, IN, USA). Poly(vinyl alcohol) (PVA, 6 kDa) was purchased from Polysciences, Inc. (Warrington, PA, USA). Folate-conjugated and amine-terminated polyethylene glycol (5 kDa, pFol) and amine-terminated methoxyl polyethylene glycol (5 kDa, mPEG) were purchased from Nanocs Inc. (New York, NY, USA). Tannic acid (TA) were purchased from Sigma-Aldrich (St. Louis, MO, USA). 1,1'-Dioctadecyl-3,3,3',3'-Tetramethylindotricarbocyanine Iodide (DiR) was purchased from Fisher Scientific (Hampton, NH). Balb/c mouse serum was purchased from Innovative research (Novi, MI, USA). Indocyanine green (ICG) was purchased from MP Biomedicals, LLC (Solon, OH, USA).

Preparation of NPs

PLGA NPs—DiR-loaded PLGA NPs (DiR/np) were prepared by the single emulsion-solvent evaporation method as previously reported.[55] Briefly, 100 mg of PLGA and 3.6 or 0.5 mg of DiR were dissolved in 10 mL dichloromethane (DCM). The polymer solution was added to 30 mL of 5% PVA solution and emulsified with a Vibra-Cell probe sonicator (Sonics, Newtown, CT, USA) at 40% amplitude with a 4s on and 2s off duty cycle for 2 min.

The emulsion was then added to 30 mL of deionized (DI) water and stirred for 2 h, followed by rotary evaporation for 30 min. DiR/np were collected by centrifugation at 33,900 g, washed two times with DI water, lyophilized with a Labconco freeze-dryer (Kansas City, MO), and stored at −20 °C. DiR/np was identified by the target dye loading (DiR$_{3.6}$/np for 3.6 wt% or DiR$_{0.5}$/np for 0.5 wt%). For flow cytometry, rhodamine-labeled PLGA NPs (np*) was prepared using a PLGA-rhodamine B conjugate (omitting DiR) and processed in the same way as DiR/np.

ICG-loaded PLGA NPs (ICG$_{0.5}$/np) were prepared by the double emulsion-solvent evaporation method. First, 50 mg of PLGA were dissolved in 5 mL DCM. A mixture of 0.75 mg of human serum albumin (HSA) and 0.25 mg of ICG was dissolved in 0.4 mL of DI water and added to PLGA solution. The mixture was emulsified by probe sonication at 40% amplitude with a 1s on and 1s off duty cycle for 2 min to form a primary emulsion, which was added to 15 mL of 5% PVA solution and processed as described above.

Surface-modification of NPs—DiR/np, np, or np* was modified with pFol or mPEG *via* polymerized tannic acid (pTA) as an intermediate adhesive layer.[27,55] To form the pTA layer, 5 μL of 40 mg/mL TA solution was added to 0.5 mL of 5 mg/mL NP suspension and vortex-mixed for 30 s. Five microliters of 10 mg/mL iron chloride solution was then added and mixed for another 30 s. The pH was adjusted to 7.4 by bicine buffer (10 mM). The pTA-coated PLGA NPs (np-pTA) were collected by centrifugation, washed with DI water, and incubated with pFol or mPEG in 1:1 weight ratio for 30 min in bicine buffer. The surface modified NPs were purified by centrifugation, washed twice with water, lyophilized, and stored at −20 °C. The NPs were called np-pTA-pFol or np-pTA-PEG according to the surface modifiers.

Characterization of NPs

Physicochemical properties of NPs—The size and zeta potential of all NPs were measured in bicine buffer (10 mM, pH 7.4) with a Malvern Zetasizer Nano ZS90 (Worcestershire, UK). NP morphology was observed by transmission electron microscopy. An NP suspension (~1 mg/mL) was spotted on a Formvar-coated carbon grid (400 mesh), negatively stained with 1% uranyl acetate, and visualized with a FEI Tecnai T20 transmission electron microscope.

Matrix-assisted laser desorption/ionization mass spectrometry (MALDI-MS)—
The presence of pFol and mPEG on np-pTA-pFol and np-pTA-PEG was confirmed by MALDI-MS analysis. np-pTA-pFol or np-pTA-PEG were dispersed in 0.1% trifluoroacetic acid at a final concentration of 1 mg/mL to dissociate pTA and release the surface-bound pFol and mPEG. After 24 h, the NPs were centrifuged at 33,000 g for 15 min to separate supernatants, which were mixed with matrix solution for MALDI-MS analysis. mPEG, pFol and np-pTA treated in the same manner were also analyzed for comparison.

Stability of NP fluorescence intensity in mouse serum—DiR/NPs (with or without surface modification) and ICG/np were dispersed in mouse serum or PBS (10 mM, pH 7.4) at specified concentrations. The NP suspension was divided into several aliquots of 200 μL

and kept at 37 °C with shaking. One aliquot was taken at each time point and centrifuged at 33,900 g for 25 min. The supernatant was collected, and the NP pellet was redispersed in 200 μL of fresh mouse serum or PBS. The supernatant and redispersed NP suspension were placed in a 96 well plate and imaged by a SPECTRAL AMI Imaging System (Spectral Instruments, Tucson, AZ) with an excitation and emission wavelength of 745 and 790 nm (for DiR/NPs) or by IVIS Lumina II Optical Imaging System (Caliper LifeSciences, Hopkinton, MA) under excitation of 745 nm and emission of ICG channel (for ICG/np). The measurements of DiR/NPs were repeated with independently prepared NPs. Due to the high sensitivity of raw fluorescence reading to slight difference in actual dye loading, the replicates were presented separately in Supporting Figures.

NP interactions with folate receptor-overexpressing KB cells—The surface functionality of NPs was evaluated based on the interaction with KB human carcinoma cells (ATCC, Manassas, VA). KB cells were seeded in a 24-well plate at a density of 50,000 cells per well and cultured overnight in folate-free RPMI 1640 medium supplemented with 10% FBS, 100 units/mL penicillin and 100 μg/mL streptomycin. KB cells were incubated with 200 μg/mL of np*-pTA-pFol or np*-pTA-PEG in complete medium. To confirm that the cell-NP interaction was mediated by the folate receptor, folic acid was added to the medium as a competitive substrate at a final concentration of 1 mM simultaneously with the NPs. The cells were collected after 2 h incubation, and their fluorescence intensities were measured by a BD Accuri C6 Flow Cytometer (BD Bioscience, Bedford, MA,USA) with an FL-2 detector ($\lambda_{Ex}/\lambda_{Em}$=550 nm/600 nm). A total of 10,000 gated events were acquired for each analysis.

In vivo and *ex vivo* imaging of NP distribution in tumor-bearing mice

All animal procedures were approved by Purdue Animal Care and Use Committee, in conformity with the NIH guidelines for the care and use of laboratory animals. 5–6 weeks old female athymic nude mouse were purchased from Envigo (Indianapolis, IN). Mice were fed with folate-deficient diet (TestDiet 1816127, Richmond, IN) for 2 weeks prior to tumor inoculation. A xenograft tumor model was prepared by subcutaneous injection of 10^7 KB cells on the upper flank of the right hind leg. The length (L) and width (W) of each tumor were measured daily with a digital caliper, and the volume (V) was calculated according to the modified ellipsoid formula: $V = (L \times W^2)/2$. When the tumor grew to 400-600 mm³, animals were treated with DiR/np-pTA-pFol or DiR/np-pTA-PEG dispersed in 200 μL of 5% dextrose by tail vein injection at the dose of 0.4 or 4 mg per mouse. Whole body images were acquired under 2.5% isoflurane anesthesia at specified times after injection by the AMI imager. After the final imaging, animals were humanely sacrificed, and major organs were collected and imaged by the AMI imager. The radiance (photon emission per unit area) of a region-of-interest (ROI) was acquired by the AMI viewer image software (Spectral Instruments, Tucson, AZ).

Liquid-liquid extraction and quantification of DiR in tissues

The collected livers and tumors were weighed and cut into small pieces using dissecting scissors. Three hundred milligrams of the tissues were homogenized in 1 mL of 5% Triton X100 solution. The tissue homogenate was extracted with ethyl acetate 3 times to isolate

DiR. The ethyl acetate phases were pooled, evaporated and redissolved in DMSO for AMI analysis. A standard curve were constructed with DiR spiked in 5% Triton X100 solution and processed in the same way. The DiR in tissue was expressed as the amount of DiR divided by tissue mass (μg/g).

Fluorescence intensity of NIR dyes in mouse serum

ICG and FPI-749 were dissolved in mouse serum in different concentrations. The fluorescence intensity of FPI-749 (Cy 7) solution was measured by the AMI imager with an excitation and emission wavelength of 745 and 790 nm. ICG solution was analyzed by IVIS Lumina II Optical Imaging Systems with an excitation wavelength of 745 nm and an emission channel for ICG.

Statistical analysis

All statistical analyses were performed with GraphPad Prism 7 (La Jolla, CA). Data were analyzed by one-way or two-way ANOVA test to determine the difference among groups, followed by the recommended multiple comparisons test. A value of $p < 0.05$ was considered statistically significant.

Supplementary Material

Refer to Web version on PubMed Central for supplementary material.

Acknowledgments

References

(1). Etrych T; Lucas H; Janoušková O; Chytil P; Mueller T; Mäder K, Fluorescence Optical Imaging in Anticancer Drug Delivery. J. Control. Release 2016, 226, 168–181. [PubMed: 26892751]

(2). Ntziachristos V; Bremer C; Weissleder R, Fluorescence Imaging with Near-Infrared Light: New Technological Advances That Enable *In Vivo* Molecular Imaging. Eur. Radiol 2003, 13, 195–208. [PubMed: 12541130]

(3). Weissleder R; Ntziachristos V, Shedding Light onto Live Molecular Targets. Nat. Med 2003, 9, 123–128. [PubMed: 12514725]

(4). Pansare VJ; Hejazi S; Faenza WJ; Prud'homme RK, Review of Long-Wavelength Optical and NIR Imaging Materials: Contrast Agents, Fluorophores, and Multifunctional Nano Carriers. Chem. Mater 2012, 24, 812–827. [PubMed: 22919122]

(5). Shi C; Wu JB; Pan D, Review on near-Infrared Heptamethine Cyanine Dyes as Theranostic Agents for Tumor Imaging, Targeting, and Photodynamic Therapy. J. Biomed. Opt 2016, 21, 50901. [PubMed: 27165449]

(6). Liu T-M; Conde J; Lipinski T; Bednarkiewicz A; Huang C-C, Revisiting the Classification of NIR-Absorbing/Emitting Nanomaterials for *In Vivo* Bioapplications. NPG Asia Mater. 2016, 8, e295.

(7). Yun SH; Kwok SJJ, Light in Diagnosis, Therapy and Surgery. Nat. Biomed. Eng 2017, 1, 0008. [PubMed: 28649464]

(8). Reisch A; Klymchenko AS, Fluorescent Polymer Nanoparticles Based on Dyes: Seeking Brighter Tools for Bioimaging. Small 2016, 12, 1968–1992. [PubMed: 26901678]

(9). Hong G; Antaris AL; Dai H, Near-Infrared Fluorophores for Biomedical Imaging. Nat. Biomed. Eng 2017, 1, 0010.

(10). Weber J; Beard PC; Bohndiek SE, Contrast Agents for Molecular Photoacoustic Imaging. Nat. Methods 2016, 13, 639. [PubMed: 27467727]

(11). Park J; Pei Y; Hyun H; Castanares MA; Collins DS; Yeo Y, Small Molecule Delivery to Solid Tumors with Chitosan-Coated PLGA Particles: A Lesson Learned from Comparative Imaging. J. Control. Release 2017, 268, 407–415. [PubMed: 29111150]

(12). Mérian J; Boisgard R; Bayle P-A; Bardet M; Tavitian B; Texier I, Comparative Biodistribution in Mice of Cyanine Dyes Loaded in Lipid Nanoparticles. Eur. J. Pharm. Biopharm 2015, 93, 1–10. [PubMed: 25805562]

(13). Benson RC; Kues HA, Fluorescence Properties of Indocyanine Green as Related to Angiography. Phys. Med. Biol 1978, 23, 159–163. [PubMed: 635011]

(14). Pansare VJ; Faenza WJ; Lu HJ; Adamson DH; Prud'homme RK, Formulation of Long-Wavelength Indocyanine Green Nanocarriers. J. Biomed. Opt 2017, 22, 11.

(15). Liu X; Li Y; Tan X; Rao R; Ren Y; Liu L; Yang X; Liu W, Multifunctional Hybrid Micelles with Tunable Active Targeting and Acid/Phosphatase-Stimulated Drug Release for Enhanced Tumor Suppression. Biomaterials 2018, 157, 136–148. [PubMed: 29268144]

(16). Guo P; Liu D; Subramanyam K; Wang B; Yang J; Huang J; Auguste DT; Moses MA, Nanoparticle Elasticity Directs Tumor Uptake. Nat. Commun 2018, 9, 130. [PubMed: 29317633]

(17). Tamura R; Uemoto S; Tabata Y, Augmented Liver Targeting of Exosomes by Surface Modification with Cationized Pullulan. Acta Biomater. 2017, 57, 274–284. [PubMed: 28483695]

(18). Ebeid K; Meng X; Thiel KW; Do A-V; Geary SM; Morris AS; Pham EL; Wongrakpanich A; Chhonker YS; Murry DJ; Leslie KK; Salem AK, Synthetically Lethal Nanoparticles for Treatment of Endometrial Cancer. Nat. Nanotechnol 2018, 13, 72–81. [PubMed: 29203914]

(19). Huang J-L; Jiang G; Song Q-X; Gu X; Hu M; Wang X-L; Song H-H; Chen L-P; Lin Y-Y; Jiang D; Chen J; Feng J-F; Qiu Y-M; Jiang J-Y; Jiang X-G; Chen H-Z; Gao X-L, Lipoprotein-Biomimetic Nanostructure Enables Efficient Targeting Delivery of siRNA to Ras-Activated Glioblastoma Cells *Via* Macropinocytosis. Nat. Commun 2017, 8, 15144. [PubMed: 28489075]

(20). Su J; Sun H; Meng Q; Yin Q; Zhang P; Zhang Z; Yu H; Li Y, Bioinspired Nanoparticles with NIR-Controlled Drug Release for Synergetic Chemophotothermal Therapy of Metastatic Breast Cancer. Adv. Funct. Mater 2016, 26, 7495–7506.

(21). Cho H; Indig GL; Weichert J; Shin H-C; Kwon GS, *In Vivo* Cancer Imaging by Poly(Ethylene Glycol)-B-Poly(Ɛ-Caprolactone) Micelles Containing a near-Infrared Probe. Nanomedicine 2012, 8, 228–236. [PubMed: 21704593]

(22). Wang H; Gao Z; Liu X; Agarwal P; Zhao S; Conroy DW; Ji G; Yu J; Jaroniec CP; Liu Z; Lu X; Li X; He X, Targeted Production of Reactive Oxygen Species in Mitochondria to Overcome Cancer Drug Resistance. Nat. Commun 2018, 9, 562. [PubMed: 29422620]

(23). Xue J; Zhao Z; Zhang L; Xue L; Shen S; Wen Y; Wei Z; Wang L; Kong L; Sun H; Ping Q; Mo R; Zhang C, Neutrophil-Mediated Anticancer Drug Delivery for Suppression of Postoperative Malignant Glioma Recurrence. Nat. Nanotechnol 2017, 12, 692. [PubMed: 28650441]

(24). Behera GB; Behera PK; Mishra BK, Cyanine Dyes: Self Aggregation and Behaviour in Surfactants. J. Surface Sci. Technol 2007, 31.

(25). Kunzler J; Samha L; Zhang R; Samha H, Investigation of the Effect of Concentration on Molecular Aggregation of Cyanine Dyes in Aqueous Solution. Am. J. Undegrad. Res 2011, 9, 1–4.

(26). Chakraborty S; Debnath P; Dey D; Bhattacharjee D; Hussain SA, Formation of Fluorescent H-Aggregates of a Cyanine Dye in Ultrathin Film and Its Effect on Energy Transfer. J. Photochem. Photobiol. A Chem. 2014, 293, 57–64.

(27). Ejima H; Richardson JJ; Liang K; Best JP; van Koeverden MP; Such GK; Cui J; Caruso F, One-Step Assembly of Coordination Complexes for Versatile Film and Particle Engineering. Science 2013, 341, 154–157. [PubMed: 23846899]

(28). Sileika TS; Barrett DG; Zhang R; Lau KHA; Messersmith PB, Colorless Multifunctional Coatings Inspired by Polyphenols Found in Tea, Chocolate, and Wine. Angew. Chem. Int. Ed. Engl 2013, 52, 10766–10770. [PubMed: 24027124]

(29). Pranantyo D; Xu LQ; Neoh KG; Kang E-T; Teo SL-M, Antifouling Coatings *Via* Tethering of Hyperbranched Polyglycerols on Biomimetic Anchors. Ind. Eng. Chem. Res 2016, 55, 1890–1901.

(30). Li J; Wu S; Wu C; Qiu L; Zhu G; Cui C; Liu Y; Hou W; Wang Y; Zhang L; Teng I. t.; Yang H-H; Tan W, Versatile Surface Engineering of Porous Nanomaterials with Bioinspired Polyphenol Coatings for Targeted and Controlled Drug Delivery. Nanoscale 2016, 8, 8600–8606. [PubMed: 27050780]

(31). Rabanel J-M; Hildgen P; Banquy X, Assessment of Peg on Polymeric Particles Surface, a Key Step in Drug Carrier Translation. J. Control. Release 2014, 185, 71–87. [PubMed: 24768790]

(32). Wagh A; Qian SY; Law B, Development of Biocompatible Polymeric Nanoparticles for *In Vivo* NIR and FRET Imaging. Bioconjug. Chem 2012, 23, 981–992. [PubMed: 22482883]

(33). Abouelmagd SA; Sun B; Chang AC; Ku YJ; Yeo Y, Release Kinetics Study of Poorly Water-Soluble Drugs from Nanoparticles: Are We Doing It Right? Mol. Pharm 2015, 12, 997–1003. [PubMed: 25658769]

(34). Maurya SK; Dutta C; Goswami D, Concentration Dependent Approach for Accurate Determination of Two-Photon Absorption Cross-Section of Fluorescent Dye Molecule. J. Fluoresc 2017, 27, 1399–1403. [PubMed: 28401413]

(35). Jonasson JK; Loren N; Olofsson P; Nyden M; Rudemo M, A Pixel-Based Likelihood Framework for Analysis of Fluorescence Recovery after Photobleaching Data. J. Microsc 2008, 232, 260–269. [PubMed: 19017225]

(36). Tang L; Tong R; Coyle VJ; Yin Q; Pondenis H; Borst LB; Cheng J; Fan TM, Targeting Tumor Vasculature with Aptamer-Functionalized Doxorubicin–Polylactide Nanoconjugates for Enhanced Cancer Therapy. ACS Nano 2015, 9, 5072–5081. [PubMed: 25938427]

(37). Guo J; Hong H; Chen G; Shi S; Zheng Q; Zhang Y; Theuer CP; Barnhart TE; Cai W; Gong S, Image-Guided and Tumor-Targeted Drug Delivery with Radiolabeled Unimolecular Micelles. Biomaterials 2013, 34, 8323–8332. [PubMed: 23932288]

(38). Pathak A; Kumar P; Chuttani K; Jain S; Mishra AK; Vyas SP; Gupta KC, Gene Expression, Biodistribution, and Pharmacoscintigraphic Evaluation of Chondroitin Sulfate–Pei Nanoconstructs Mediated Tumor Gene Therapy. ACS Nano 2009, 3, 1493–1505. [PubMed: 19449835]

(39). Wilhelm S; Tavares AJ; Dai Q; Ohta S; Audet J; Dvorak HF; Chan WCW, Analysis of Nanoparticle Delivery to Tumours. Nat. Rev. Mater 2016, 1, 16014.

(40). Shalgunov V; Zaytseva-Zotova D; Zintchenko A; Levada T; Shilov Y; Andreyev D; Dzhumashev D; Metelkin E; Urusova A; Demin O; McDonnell K; Troiano G; Zale S; Safarova E, Comprehensive Study of the Drug Delivery Properties of Poly(L-Lactide)-Poly(Ethylene Glycol) Nanoparticles in Rats and Tumor-Bearing Mice. J. Control. Release 2017, 261, 31–42. [PubMed: 28611009]

(41). Yu T; Hubbard D; Ray A; Ghandehari H, *In Vivo* Biodistribution and Pharmacokinetics of Silica Nanoparticles as a Function of Geometry, Porosity and Surface Characteristics. J. Control. Release 2012, 163, 46–54. [PubMed: 22684119]

(42). Song Z; , R. F; , M. S; , C. G; , Y. G; , L. L; , G. Z, Curcumin-Loaded PLGA-PEG-PLGA Triblock Copolymeric Micelles: Preparation, Pharmacokinetics and Distribution *In Vivo*. J. Colloid Interface Sci 2011, 254, 116–123.

(43). Li K; Liu B, Polymer-Encapsulated Organic Nanoparticles for Fluorescence and Photoacoustic Imaging. Chem. Soc. Rev 2014, 43, 6570–6597. [PubMed: 24792930]

(44). Escobedo JO; Rusin O; Lim S; Strongin RM, NIR Dyes for Bioimaging Applications. Curr. Opin. Chem. Biol 2010, 14, 64–70. [PubMed: 19926332]

(45). Guosong H; T. RJ; Yejun Z; Shuo D; L. AA; Qiangbin W; Hongjie D, *In Vivo* Fluorescence Imaging with Ag2s Quantum Dots in the Second Near-Infrared Region. Angew. Chem. Int. Ed. Engl 2012, 51, 9818–9821. [PubMed: 22951900]

Author Manuscript

Author Manuscript

Author Manuscript

Author Manuscript

(46). Wegner KD; Hildebrandt N, Quantum Dots: Bright and Versatile *In Vitro* and *In Vivo* Fluorescence Imaging Biosensors. Chem. Soc. Rev 2015, 44, 4792–4834. [PubMed: 25777768]

(47). Yang S-T; Cao L; Luo PG; Lu F; Wang X; Wang H; Meziani MJ; Liu Y; Qi G; Sun Y-P, Carbon Dots for Optical Imaging *In Vivo*. J. Am. Chem. Soc 2009, 131, 11308–11309. [PubMed: 19722643]

(48). Resch-Genger U; Grabolle M; Cavaliere-Jaricot S; Nitschke R; Nann T, Quantum Dots *Versus* Organic Dyes as Fluorescent Labels. Nat. Methods 2008, 5, 763. [PubMed: 18756197]

(49). Kumar V; Adamson DH; Prud'homme RK, Fluorescent Polymeric Nanoparticles: Aggregation and Phase Behavior of Pyrene and Amphotericin B Molecules in Nanoparticle Cores. Small 2010, 6, 2907–2914. [PubMed: 21104798]

(50). Genovese D; Rampazzo E; Bonacchi S; Montalti M; Zaccheroni N; Prodi L, Energy Transfer Processes in Dye-Doped Nanostructures Yield Cooperative and Versatile Fluorescent Probes. Nanoscale 2014, 6, 3022–3036. [PubMed: 24531884]

(51). Ng KK; Zheng G, Molecular Interactions in Organic Nanoparticles for Phototheranostic Applications. Chem. Rev 2015, 115, 11012–11042. [PubMed: 26244706]

(52). Park K; Lee S; Kang E; Kim K; Choi K; Kwon IC, New Generation of Multifunctional Nanoparticles for Cancer Imaging and Therapy. Adv. Funct. Mater 2009, 19, 1553–1566.

(53). Kobayashi H; Ogawa M; Alford R; Choyke PL; Urano Y, New Strategies for Fluorescent Probe Design in Medical Diagnostic Imaging. Chem. Rev 2010, 110, 2620–2640. [PubMed: 20000749]

(54). Bremer C; Tung C-H; Weissleder R, *In Vivo* Molecular Target Assessment of Matrix Metalloproteinase Inhibition. Nat. Med 2001, 7, 743. [PubMed: 11385514]

(55). Abouelmagd SA; Meng F; Kim B-K; Hyun H; Yeo Y, Tannic Acid-Mediated Surface Functionalization of Polymeric Nanoparticles. ACS Biomater. Sci. Eng 2016, 2, 2294–2303. [PubMed: 28944286]
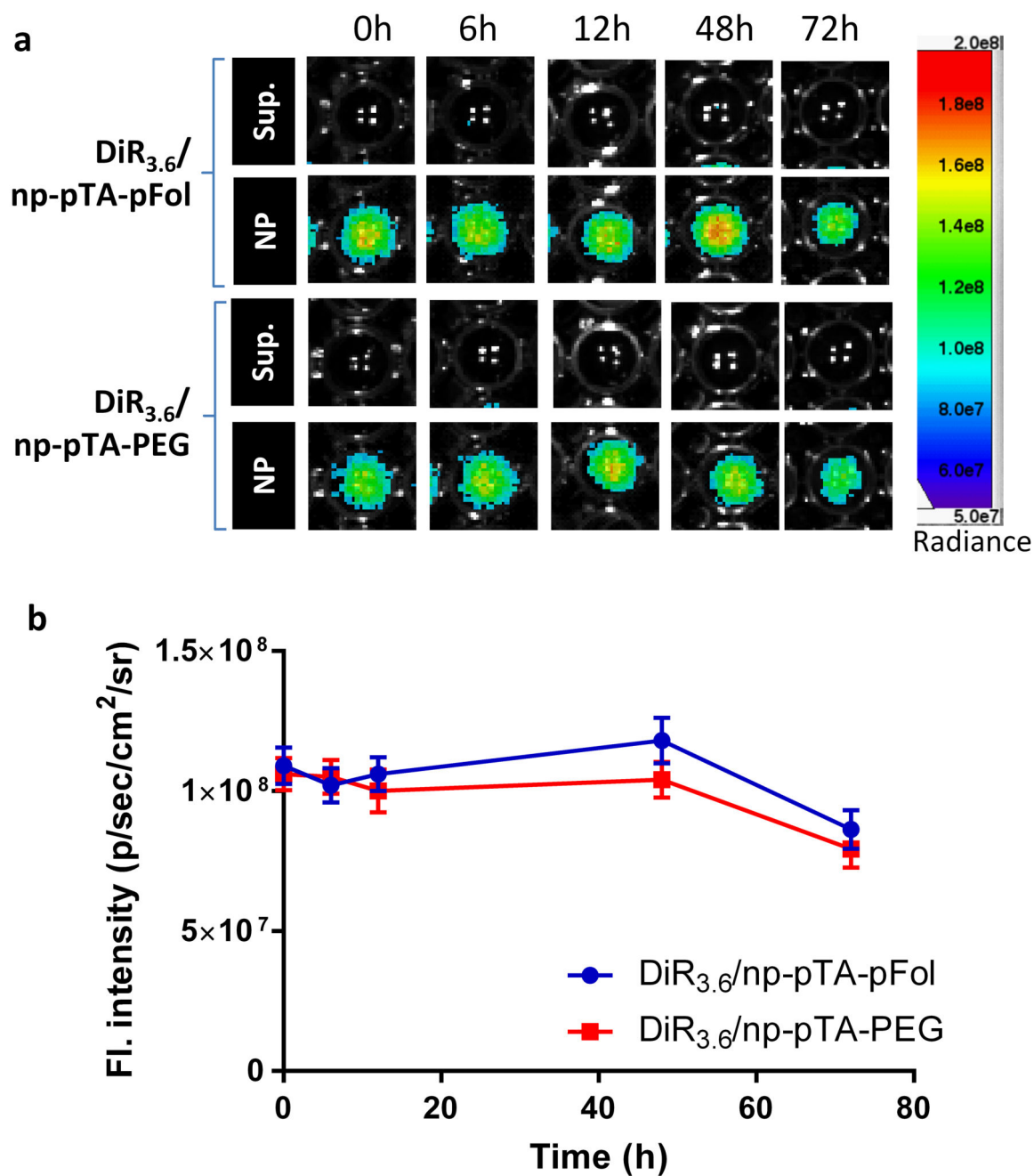
Fig. 1.
Stability of $DiR_{3.6}$/np-pTA-pFol and $DiR_{3.6}$/np-pTA-PEG in mouse serum (NPs: 1 mg/mL, DiR loading: 3.6%). (a) Fluorescence images of supernatants and NPs (redispersed in fresh mouse serum) collected at different time points during the incubation in mouse serum. (b) Fluorescence intensity of the NPs collected at the specified time points and redispersed in fresh mouse serum, quantified by the AMI viewer image software. Error bars: s.d. of 3 readings of the same sample in a representative experiment. The measurement was repeated with an independently prepared batch of NPs (Fig. S7).
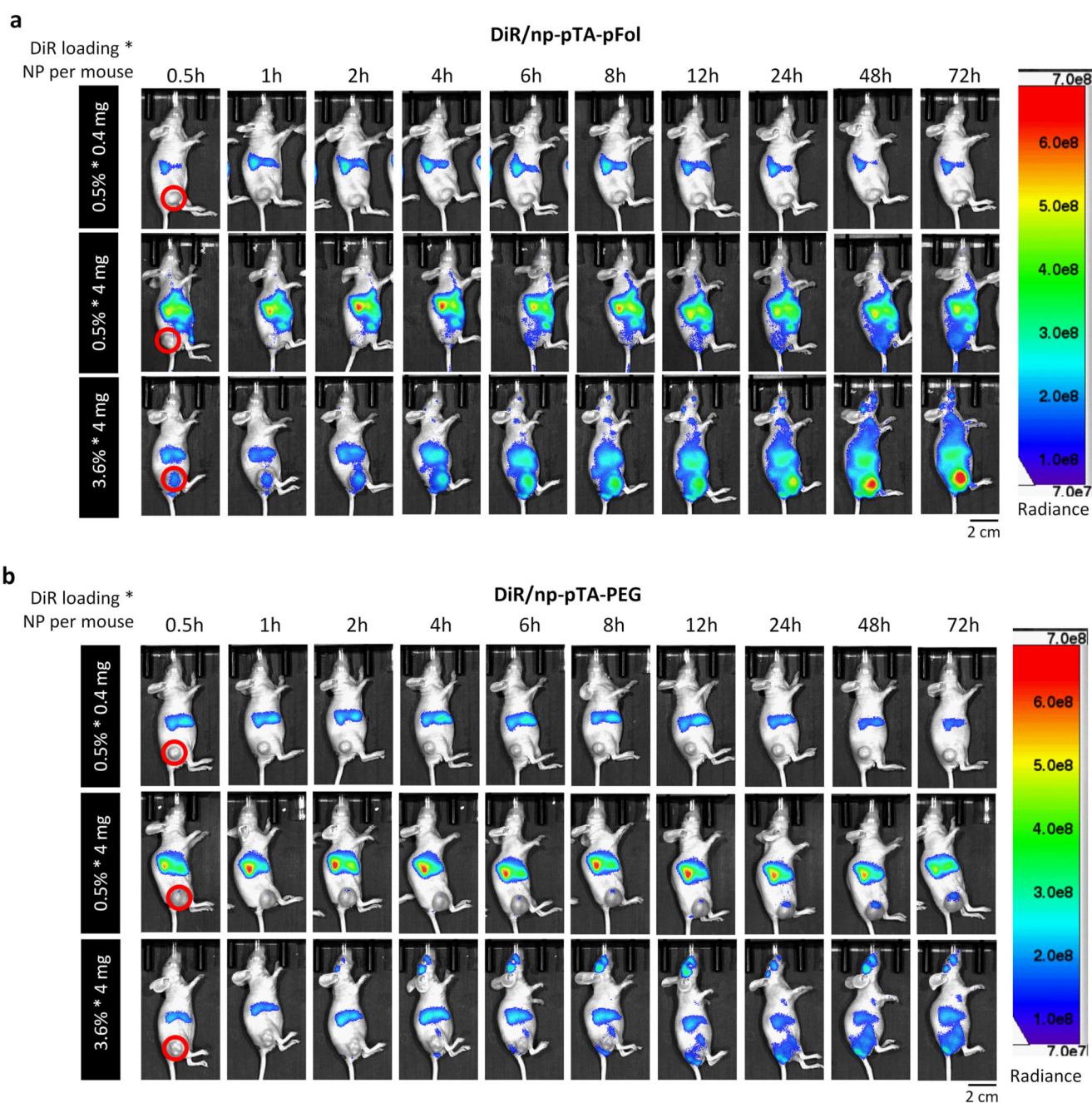
Fig. 2.

Real-time whole body imaging of KB tumor-bearing female nude mice at different time points after tail vein injection of (a) DiR/np-pTA-pFol or (b) DiR/np-pTA-PEG with different DiR loading (0.5 or 3.6%) at NP doses of 0.4 or 4 mg per mouse. Red solid circles indicate subcutaneous KB tumors. Only tumor-bearing side (right) is shown. For all sides, see Figure S8. The experiment was repeated with three independently prepared batches of NPs at selected levels of NP dose and dye loading and presented in Fig. S9, S12, and S15.
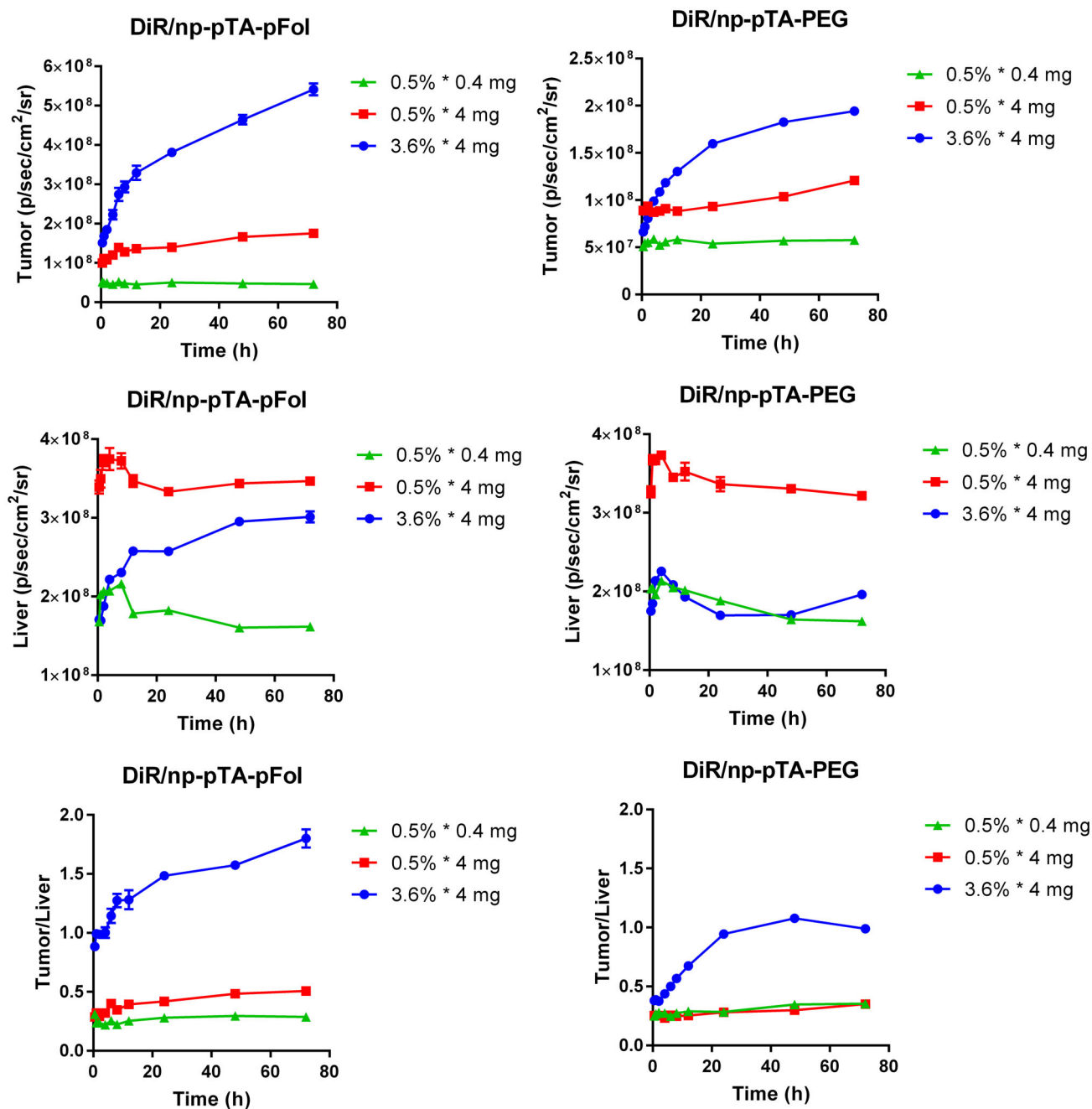
Fig. 3.

Fluorescence intensity of tumor and liver *in situ* and their ratio after tail vein injection of (left) DiR/np-pTA-pFol or (right) DiR/np-pTA-PEG. The fluorescence intensity of region of interest (ROI) was quantified by the AMI viewer image software and expressed as radiance ($p/sec/cm^2/sr$). Error bars: s.d. of 3 readings of the same subject. The experiment was repeated with three independently prepared batches of NPs at selected levels of NP dose and dye loading and presented in S10, S13, and S16.
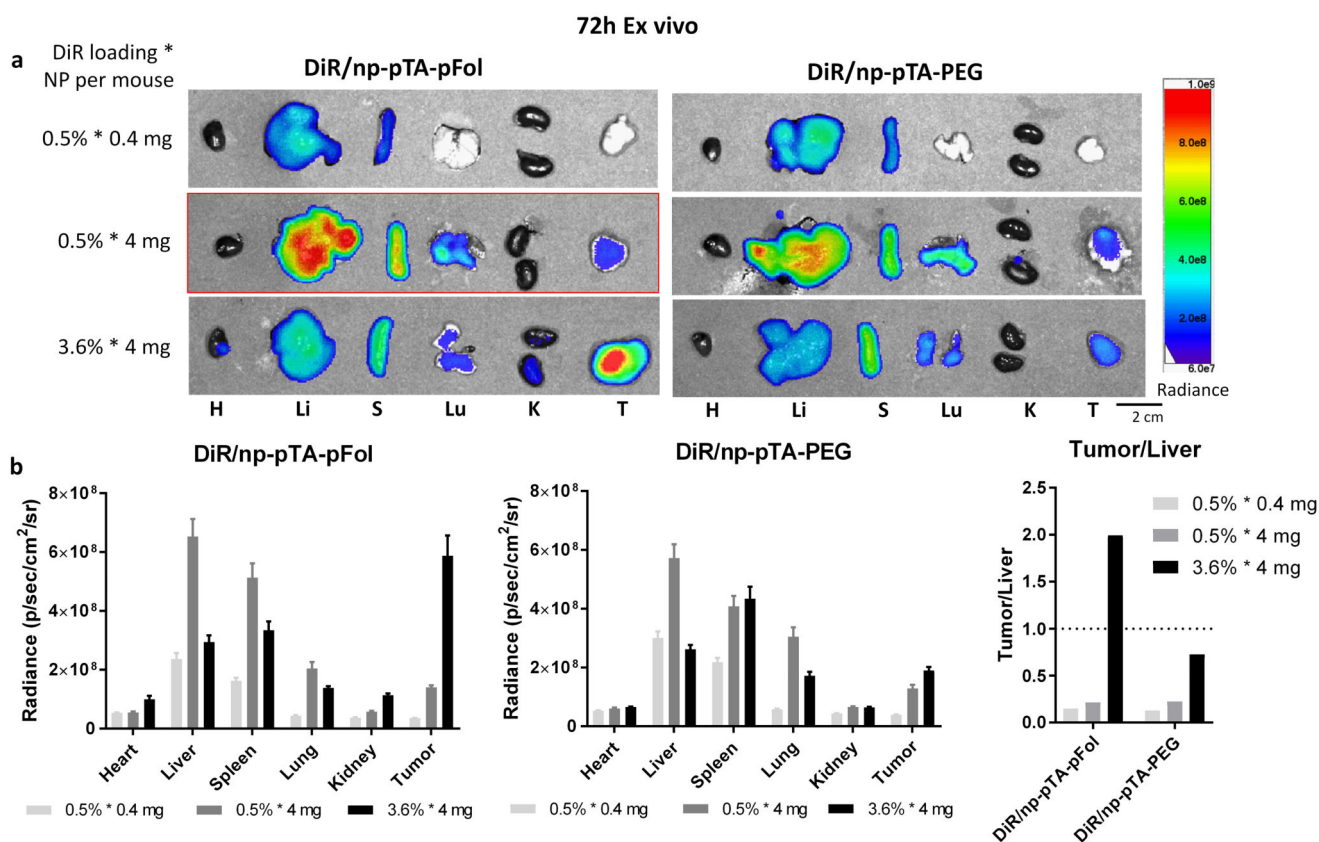
Fig. 4.

(a) Fluorescence images, (b) signal intensity of major organs and tumor/liver ratio of the signals acquired *ex vivo* at 72 h post-injection of DiR/np-pTA-pFol or DiR/np-pTA-PEG. H: heart; Li: liver; S: spleen; Lu: lung; K: kidneys; T: KB tumor. The fluorescence intensity of ROI was quantified by the AMI viewer image software and expressed as radiance $(p/sec/cm^2/sr)$. Error bars: s.d. of 3 readings of the same subject. The experiment was repeated with three independently prepared batches of NPs at selected levels of NP dose and dye loading and presented in Fig. S11, S14, and S17.
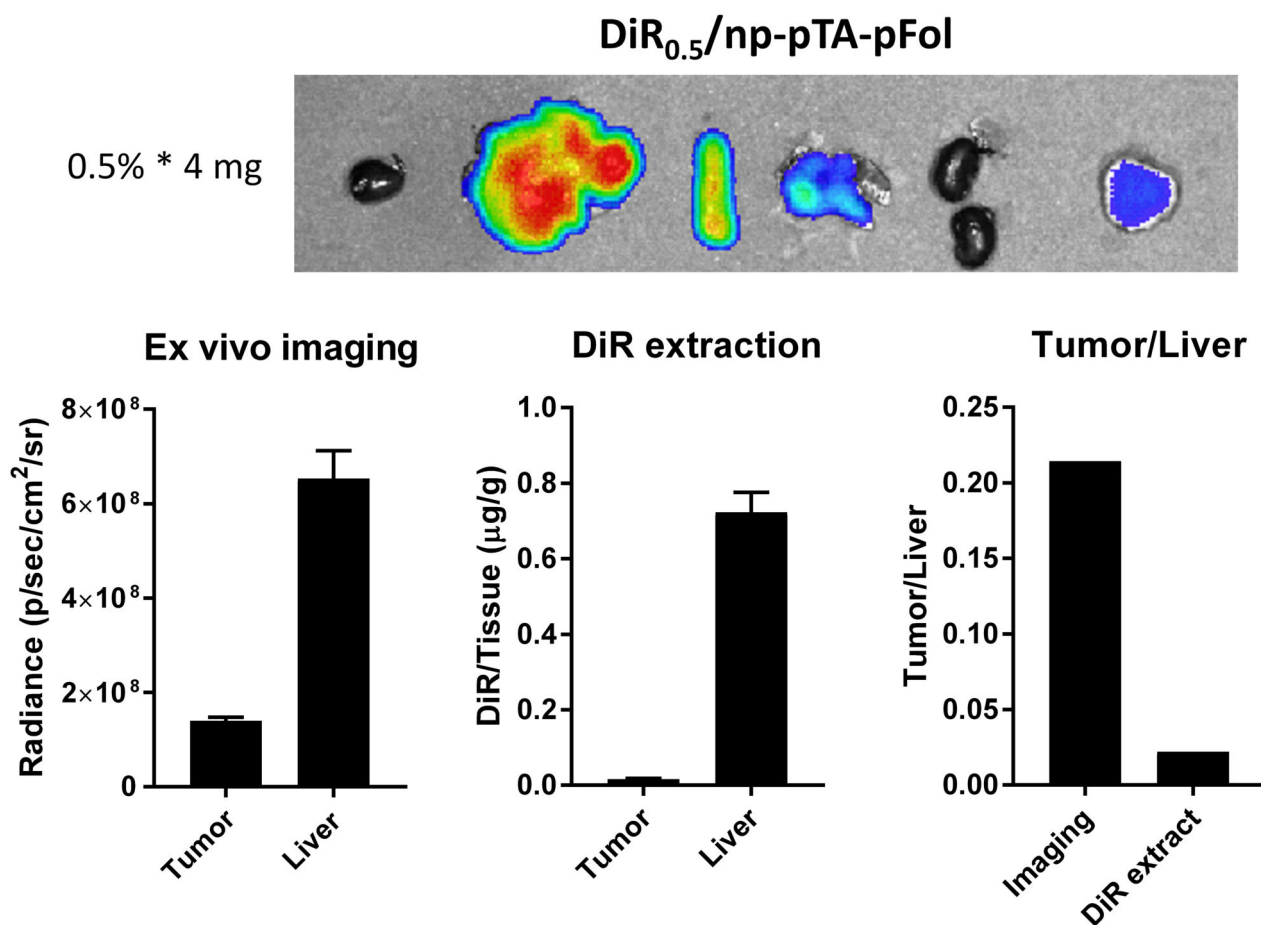
Fig. 5.

Comparison of fluorescence signals of tumor and liver and their ratios quantified by *ex vivo* fluorescence image analysis and by liquid-liquid extraction. Images and organ samples were obtained from a mouse receiving 4 mg of $DiR_{0.5}$/np-pTA-pFol at 72 h after tail vein injection. Error bars: s.d. of 3 readings of the same subject. The experiment was repeated with an independently prepared batch of NPs and presented in Fig. S18.
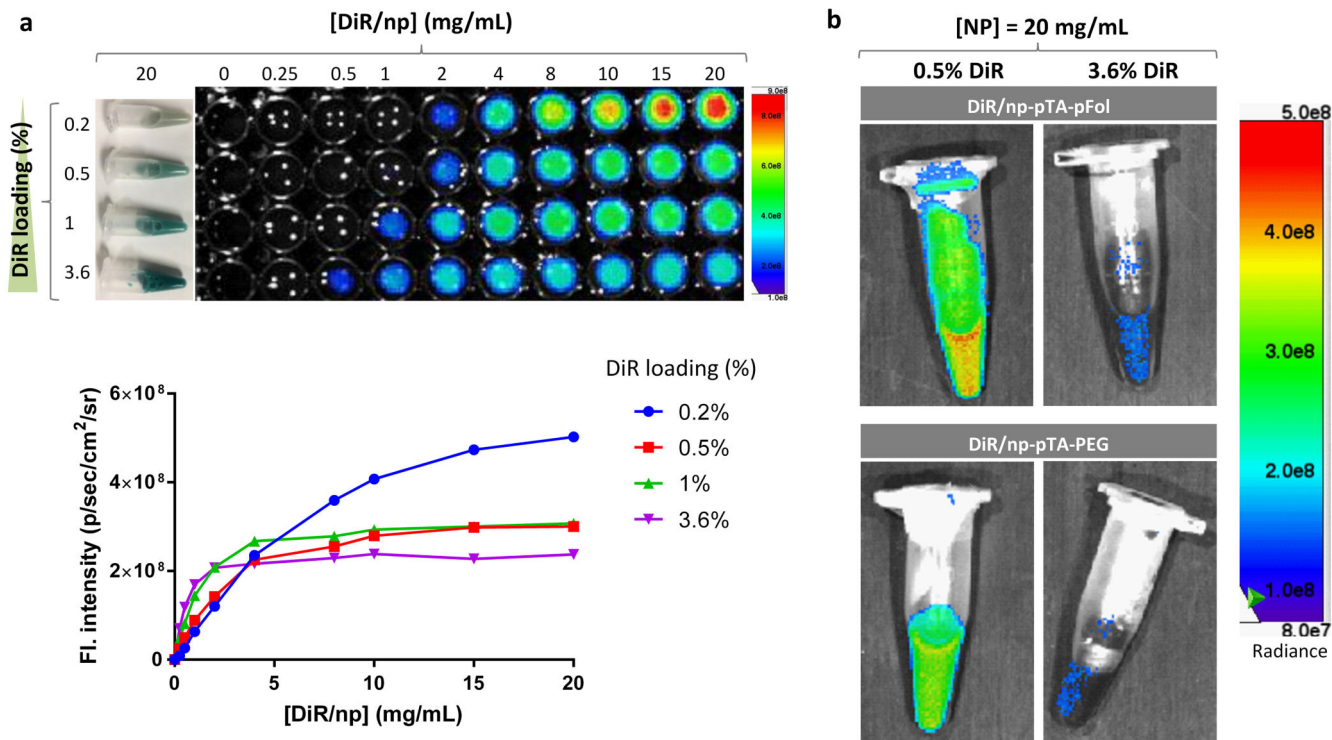
Fig. 6.

(a) Fluorescence intensity *vs.* concentration of DiR-loaded PLGA NPs (DiR/np) with different dye loading. Top: Photographic images of DiR/np suspended in mouse serum at 20 mg/mL are shown on the left, and fluorescence images of DiR/np at different concentrations shown on the right. Bottom: The fluorescence intensity was quantified by the SPECTRAL AMI Imaging System. The measurement was repeated with the same batch NPs (Fig. S19a) or an independently prepared batch of NPs (Fig. S19b). (b) Fluorescence images of DiR/np-pTA-pFol and DiR/np-pTA-PEG with different DiR loading, suspended in PBS at 20 mg/mL.
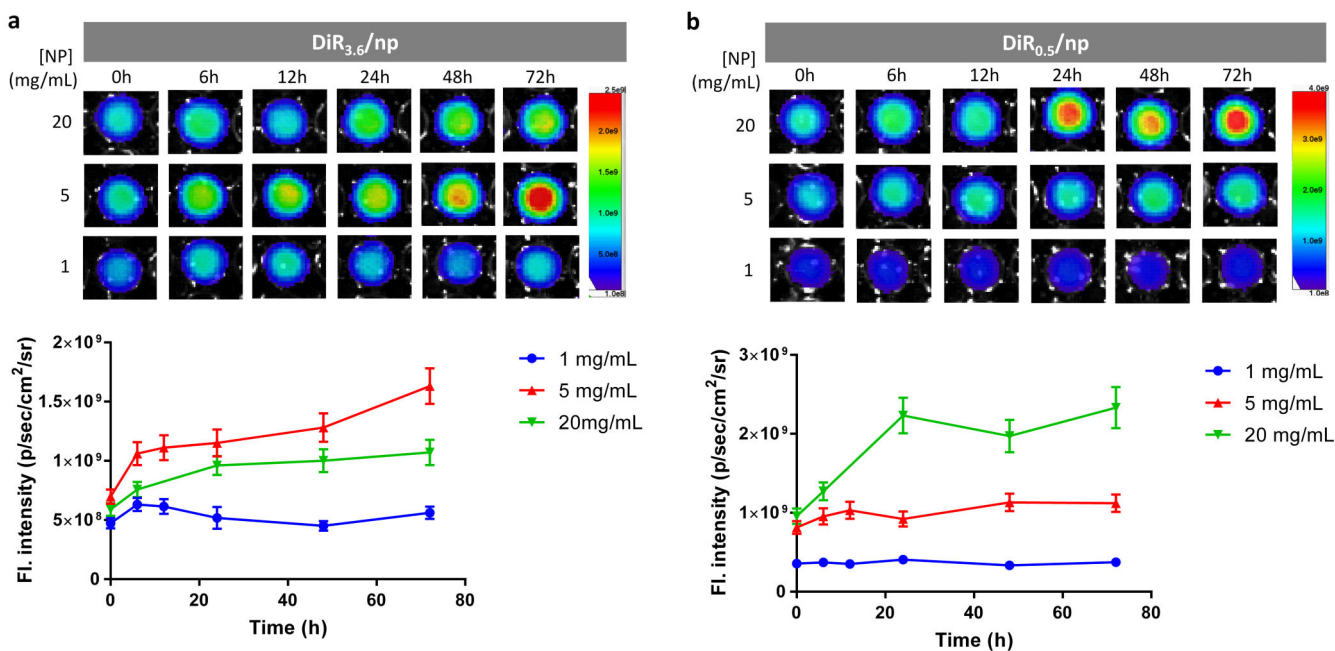
Fig. 7.
Fluorescence intensity of DiR/np with different DiR loading suspended in mouse serum at different NP concentrations, observed at different time points. (a) $DiR_{3.6}$/np and (b) $DiR_{0.5}$/np. The fluorescence intensity was quantified by the SPECTRAL AMI Imaging System. Error bars: s.d. of 3 readings of the same sample. The measurement was repeated with two independently prepared batches of NPs at selected concentrations and presented in Fig. S21 and Fig. S22.